Research on Chemical Intermediates (2021) 47:235–248
https://doi.org/10.1007/s11164-020-04332-3

Why Ca_2NH works as an efficient and stable support of Ru catalyst in ammonia synthesis

Masaaki Kitano[1,2] · Kyosuke Yamagata[1] · Hideo Hosono[1,3]

Received: 13 October 2020 / Accepted: 22 October 2020 / Published online: 5 January 2021

Abstract

Hydride-based materials have recently attracted attention because of their significant promotion effect on transition metal catalysts in ammonia synthesis under mild conditions. Here, we clarify the effect of hydride-nitride, Ca_2NH, on the activity and stability of Ru catalyst as a catalyst support for ammonia synthesis. The anionic electrons formed at H^- ion vacancy sites in Ca_2NH effectively promote the N_2 dissociation over Ru surface, which accounts for the high catalytic performance with a low apparent activation energy. The catalytic activity of Ru/Ca_2NH is much superior to those of Ru/C12A7:e^-, Ru/Sr_2NH, and Ru/CaNH. The simple metal hydride, CaH_2, with Ru exhibits higher catalytic performance than Ru/Ca_2NH, but its stability is poor because weak Ru-CaH_2 interaction causes aggregation of Ru nanoparticles during the reaction. On the other hand, Ru nanoparticles are anchored on Ca_2NH surface through a strong Ru–N interaction, which leads to excellent stability of Ru/Ca_2NH catalyst.

Keywords Ca_2NH · Ammonia synthesis · Ru catalyst · Hydride

Introduction

Artificial ammonia synthesis from N_2 and H_2 gases using heterogeneous catalyst is the key technology for production of synthetic fertilizer and nitrogen-containing chemicals. Industrial process (so-called Haber–Bosch process) is conducted using

✉ Masaaki Kitano
kitano.m.aa@m.titech.ac.jp

✉ Hideo Hosono
hosono@mces.titech.ac.jp

[1] Materials Research Center for Element Strategy, Tokyo Institute of Technology, 4259 Nagatsuta Midori-ku, Yokohama 226-8503, Japan

[2] Precursory Research for Embryonic Science and Technology (PRESTO), Japan Science and Technology Agency (JST), 4-1-8 Honcho, Saitama, Kawaguchi 332-0012, Japan

[3] wpi-MANA, National Institute for Materials Science, Ibaraki, Tsukuba 305-0044, Japan

Fe-based catalyst at high temperature (400–500 °C) and pressure (10–30 MPa) to obtain high NH_3 yield (ca. 20%) [1] because efficient N_2 dissociation requires high temperature from the kinetic point of view whereas NH_3 yield is limited at high temperatures by thermodynamic equilibrium. Although more than 100 years have passed since the establishment of Haber–Bosch process, ammonia synthesis under low temperature and pressure conditions still presents a major challenge [2]. To date, Ru-based catalysts have been well studied as the second-generation catalyst for NH_3 synthesis.[3–8] In many cases, Ru nanoparticles are dispersed on carbon or metal-oxide surface and alkali or alkaline earth compounds are added as electronic promoters [9]. These alkali-promoted Ru-based catalysts show high activity at lower temperatures and pressures than Fe-based catalyst. While the alkali-promoters significantly enhance the activity of Ru catalysts, the energy barrier for N_2 cleavage cannot be reduced, resulting in a high apparent activation energy (80–120 kJ mol^{-1}). Additionally, the reaction rate of NH_3 synthesis over these Ru catalysts is retarded by strong hydrogen adsorption on Ru surface especially at low reaction temperatures [5, 10]. These are common drawbacks of Ru-based catalysts in NH_3 synthesis.

Recently, 12CaO $7Al_2O_3$ electride (C12A7:e^-) with 0-dimensional electron confinement and Ca_2N with 2D-confinement were demonstrated to promote the activity of Ru effectively at low reaction temperatures [11–14]. These catalysts enable a significant reduction in activation energy for N_2 dissociation (50–60 kJ mol^{-1}). Anionic electrons with low work function nature (2.3–2.4 eV) in these supports are transferred to the supported Ru nanoparticles, which in turn facilitates N_2 dissociation on Ru, shifting the bottleneck of ammonia synthesis from the N_2 dissociation to the formation of N-H_n species [12]. Furthermore, both Ru/C12A7:e^- and Ru/Ca_2N catalysts have reversible hydrogen absorption–desorption characteristics and this property prevents the hydrogen poisoning on Ru surface.

In the present study, we focused on the promotion effect of Ca_2N on the NH_3 synthesis activity of Ru catalyst in comparison with various nitride materials. The role of lattice hydrogen and nitrogen in Ca_2N was elucidated by isotope-labelling experiments. Ru/Ca_2N exhibits higher catalytic performance than Ru/Sr_2N with the same crystal structure and similar hydrogen-storage capability. Moreover, CaH_2, the simplest hydride, was found to function as an efficient electronic promoter for Ru catalyst in NH_3 synthesis. Not only the catalytic performance but also the stability of Ru/CaH_2 and Ru/Ca_2N were discussed on the basis of metal-support interaction.

Experimental

Materials

Ca_2N powder was prepared by the conventional solid-state reaction as the following procedure. First, Ca_3N_2 powder was mixed with Ca metal shots at a molar ratio of 1:1 and the mixture was pressed into a pellet form. The pellet covered with molybdenum foil was heated at 800 °C for 50 h in an evacuated silica tube. Then, the silica tube was rapidly quenched by water. The obtained sample was ground into a powder in an Ar-filled glovebox. As a reference sample, Ca_2NH was synthesized

by heating at 300 °C of Ca_2N powder in a flow of N_2 and H_2 (N_2:H_2 = 1:3, flow rate = 60 ml min^{-1}, pressure = 0.1 MPa) and CaNH was prepared by the heat treatment of Ca_3N_2 at 600 °C in N_2 and H_2 gas mixture (flow condition is the same as the above). Sr_2N was synthesized by heating Sr metal at 700 °C for 10 h under N_2 gas flow. CaH_2, SrH_2, and BaH_2 were prepared by heating each alkaline earth metal at 400 °C (for CaH_2) or 300 °C (for SrH_2 and BaH_2) for 10 h under high pressure H_2 atmosphere (2 MPa).

Ru-loading was carried out by heating a mixture of the sample powder and $Ru_3(CO)_{12}$ in an evacuated silica tube with the following temperature programme: 2 °C min^{-1} up to 40 °C, hold for 1 h; in 2 h up to 70 °C, hold for 1 h; in 2 h up to 120 °C, hold for 1 h; and in 2.5 h up to 250 °C, hold for 2 h; cooling down to ambient temperature. The amount of Ru-loading was fixed to 2 wt%.

Catalytic reaction

Ammonia synthesis was conducted using 0.1 g of catalyst powder in a fixed bed flow system with a synthesis gas (H_2: N_2 = 3: 1) flow rate of 60 ml min^{-1} at 0.1 MPa. The produced ammonia was trapped by in a 5-mM sulfuric acid solution, and the amount of NH_4^+ generated in the solution was determined by ion chromatography (Prominence, Shimadzu) with a conductivity detector.

Ammonia synthesis from N_2 and D_2 (or $^{15}N_2$ and H_2) was conducted using a U-shaped glass reactor connected to a closed gas circulation system. The mixture gases (total pressure: 60 kPa, N_2 (or $^{15}N_2$): D_2 (or H_2) = 1:3) was introduced into the glass system. The change in the composition of the circulating gas was monitored with a quadrupole mass spectrometer (M-101QA-TDM, Canon Anelva Corp.) and Ar was used as a carrier gas. The circulating pump placed in the system removes diffusional and adsorption/desorption limitations. The m/z = 2, 3, 4, 16, 17, 18, 19, 20, 28, and 30 masses were monitored as a function of time to follow the reaction. ND_3 (m/z = 20) was hardly detectable because it overlaps with a fragment of Ar (m/z = 20). N_2 isotopic exchange reaction was also conducted using a U-shaped glass reactor in the same way as aforementioned procedure. The mixture of $^{15}N_2$ and $^{14}N_2$ gases (total pressure: 20.0 kPa, $^{15}N_2$: $^{14}N_2$ = 1:4) was used for this reaction. The masses 28, 29 and 30 m/z were monitored as a function of time to follow the exchange.

Characterization

The crystal structure was identified by X-ray diffractometry (XRD) using a D8 Advance diffractometer (Bruker) with monochromated Cu Kα radiation (λ = 0.15418 nm). N_2 adsorption − desorption isotherms were measured at 77 K using a specific surface area analyzer (BELSORP-mini II, MicrotracBEL) to determine the Brunauer − Emmett − Teller (BET) specific surface area of samples. Raman spectra of the samples were measured with a spectrometer (HR-800, Horiba Jobin Yvon Co. Ltd., Japan) using a laser with a wavelength of 457.4 nm.

Temperature-programmed absorption (TPA) of H_2 was carried out using a catalyst analyzer (BELCAT-A, MicrotracBEL, Japan). The sample (~100 mg) was heated (1 °C min^{-1}) in a stream of 4.8% H_2/Ar mixture, and the consumption of H_2 was monitored by a thermal conductivity detector (TCD) and mass spectrometer (Bell Mass, MicrotracBEL, Japan). Temperature-programmed desorption (TPD) of H_2 was performed using the same instrument as TPA experiment. Prior to the TPD measurements, the sample was heated under a mixture of H_2 and N_2, H_2:N_2 = 3:1, 60 ml min^{-1}, 0.1 MPa, 340 °C, 10 h, which are the same reaction condition as those used for ammonia synthesis. After cooling to room temperature, the sample was placed into a TPD glass reactor in an Ar-filled glovebox. The sample was then heated (1 °C min^{-1}) in an Ar stream (30 mL min^{-1}), and the concentration of H_2 was monitored by a thermal conductivity detector (TCD) and mass spectrometer (Bell Mass, MicrotracBEL, Japan). TEM (JEM-2010F, Jeol) images of the samples were obtained to determine the microstructural characteristics.

Results and discussion

Catalytic performance of Ru loaded $Ca_2N:e^-$

Dicalcium nitride, Ca_2N, is reported to be a two-dimensional (2D) electride in which electrons are confined between positively charged layers of $[Ca_2N]^+$ with an interlayer spacing of 0.4 nm [15]. Its chemical formula can be expressed as $[Ca_2N]^+ \cdot e^-$ (denoted as $Ca_2N:e^-$). The open layered-structure provided anisotropic electrical properties (in-plane and out-of-plane work functions = 2.6 and 3.4 eV, respectively) with superior electron concentration ($N_e = \sim 1.37 \times 10^{22}$ cm^{-3}) than C12A7:e^- ($N_e = \sim 2.3 \times 10^{21}$ cm^{-3}) [15, 16]. Accordingly, Ru-loaded $Ca_2N:e^-$ is expected to function as an efficient catalyst for NH_3 synthesis as with Ru/C12A7:e^- catalyst.

Figure 1 shows powder X-ray diffraction (XRD) patterns for Ca_3N_2, $Ca_2N:e^-$ and Ru/$Ca_2N:e^-$ after NH_3 synthesis reaction. The broad diffraction patterns observed around 2Θ = 20 are not due to sample but to an X-ray transmitting capsule to protect

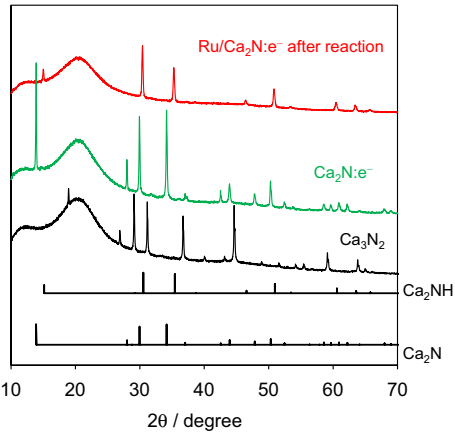

Fig. 1 XRD patterns for Ca_3N_2, $Ca_2N:e^-$, and Ru/$Ca_2N:e^-$ after ammonia synthesis at 340 °C for 20 h. Standard diffraction patterns for Ca_2N (space group R3m, PDF: 70–4196) and Ca_2NH (space group Fd3m, PDF: 76-608) are provided for reference

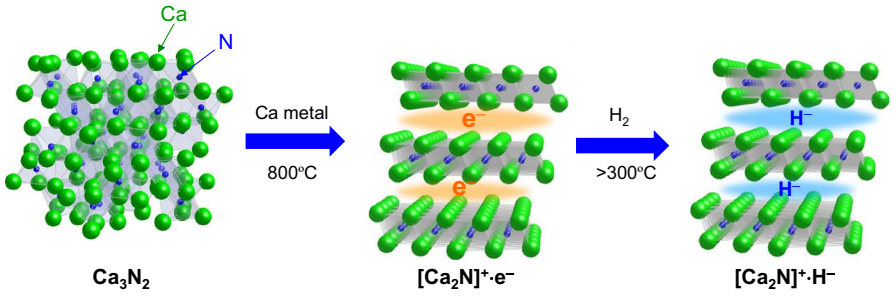

Fig. 2 Schematic illustration of structural conversion from Ca_3N_2 to $Ca_2N{:}e^-$ and Ca_2NH

sample from oxidation. The $Ca_2N{:}e^-$ with a rhombohedral layered structure is synthesized by the solid-state reaction with α–Ca_3N_2 powder and Ca metal at 800 °C in vacuum (Fig. 2) according to the following equation: $Ca_3N_2 + Ca \rightarrow 2Ca_2N$. The Ca_2N phase disappeared in $Ru/Ca_2N{:}e^-$ after NH_3 synthesis, whereas new diffraction peaks arising from the Ca_2NH phase appeared (Fig. 1). The Ca_2NH formation is attributed to the open layered-structure of $Ca_2N{:}e^-$, i.e., hydrogen species spilled over from Ru surface easily enter between the layers and react with anionic electrons to form $[Ca_2N]^+{\cdot}H^-$ (Fig. 2). For instance, the H^- ion content of Ru/Ca_2NH reached 10.6 mmol g^{-1} after ammonia synthesis reaction at 340 °C for 10 h, which means that all electrons in Ca_2N layers are replaced by H^- ions because the theoretical amount of electrons in $Ca_2N{:}e^-$ is 10.5 mmol g^{-1}.[14] This result is contrary to the case of $Ru/C12A7{:}e^-$, where only 1% of electrons are replaced with H^- ions during NH_3 synthesis at 360 °C because anionic electrons are confined in the cage composed of Ca-O and Al-O bonds [12]. Thus, the formation of $C12A7{:}H^-$ is restricted to only surface and near-surface region in $C12A7{:}e^-$.

Raman spectroscopy also confirmed that Ca_2NH, an inorganic nitride-hydride, is formed in the $Ru/Ca_2N{:}e^-$ catalyst during the NH_3 synthesis reaction (Fig. 3). Two

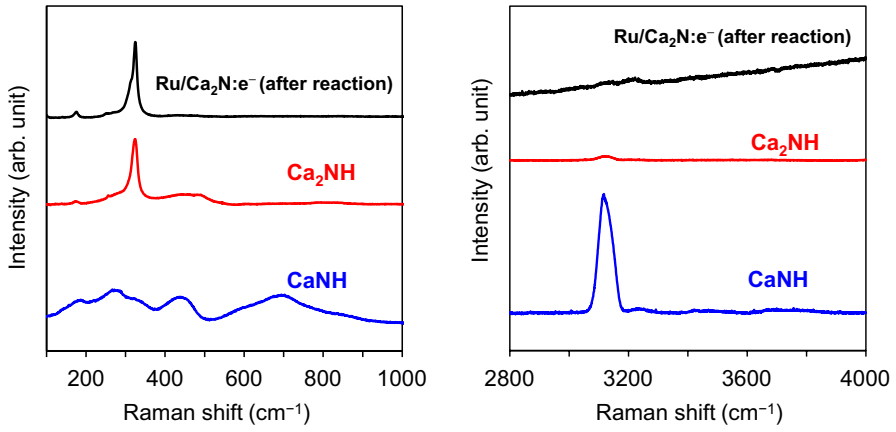

Fig. 3 Raman spectra of CaNH, Ca_2NH, and $Ru/Ca_2N{:}e^-$ after ammonia synthesis at 340 °C for 20 h

sharp peaks were observed at 177 and 326 cm^{-1} for Ca_2NH and used $Ru/Ca_2N:e^-$ catalyst, whereas several broad bands appeared in the rage of 100–1000 cm^{-1} for CaNH. The CaNH is composed of Ca^{2+} and NH^{2-} ions, i.e., the formal charge of hydrogen is + 1. Indeed, CaNH has an intense band centered at 3122 cm^{-1}, which is attributed to the N–H stretching mode in imide ions [17–19]. On the other hand, N–H band is negligibly small for the used $Ru/Ca_2N:e^-$ catalyst which was converted to Ca_2NH, indicating that the hydrogen is formally present as hydride (H^-) ion. Hereafter, the $Ru/Ca_2N:e^-$ catalyst is denoted as Ru/Ca_2NH.

Figure 4a shows the NH_3 synthesis activity of various Ru (2wt%) catalysts as a function of reaction temperature at atmospheric pressure. Ru/Ca_2NH exhibited much higher NH_3 synthesis rate than $Ru/C12A7:e^-$ and the activity was confirmed even at 200 °C. Accordingly, the apparent activation energy of Ru/Ca_2NH for NH_3 synthesis is 60 kJ mol^{-1}, which is comparable to that of $Ru/C12A7:e^-$ (50 kJ mol^{-1}). In contrast, Ru/CaNH showed low catalytic activity with a high apparent activation energy (110 kJ mol^{-1}). Thus, Ca_2NH support serves as strong electron donor to the Ru nanoparticles, reducing the energy barrier for NH_3 synthesis over Ru/Ca_2NH. Role of

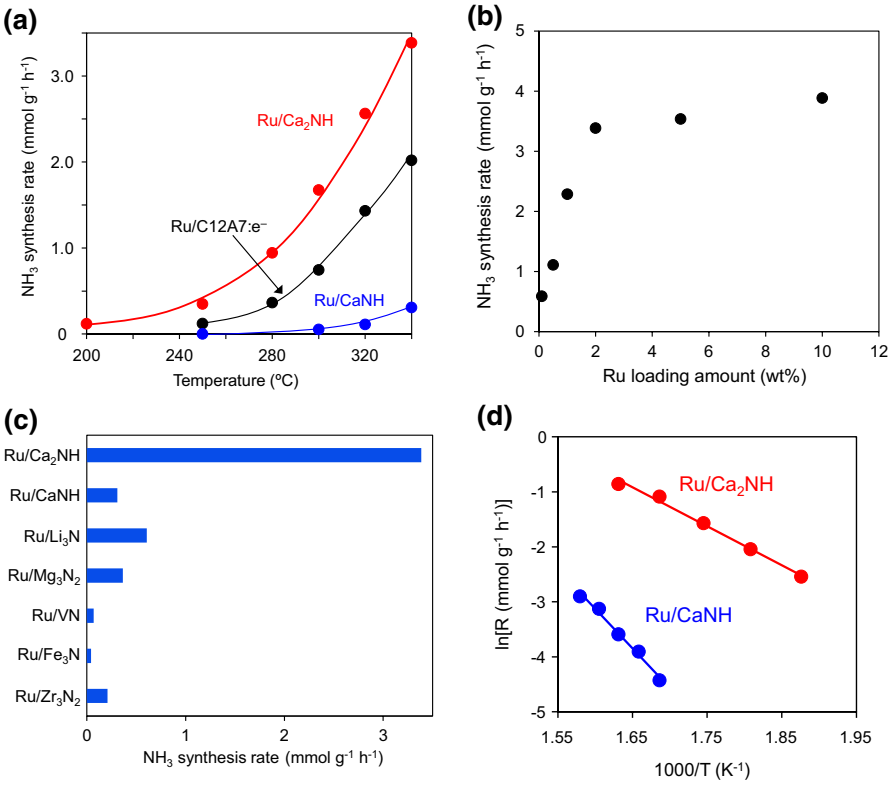

Fig. 4 **a** Temperature dependence of the rate of NH_3 synthesis over various Ru catalysts at 0.1 MPa (WHSV, 36,000 mL g_{cat}^{-1} h^{-1}). **b** NH_3 synthesis rate for Ru/Ca_2NH at 340 °C and 0.1 MPa as a function of Ru-loading amount. **c** NH_3 synthesis rate for various nitride supported Ru catalysts. **d** Arrhenius plots for N_2 isotopic exchange reaction over various Ru catalysts

loaded Ru promotes the formation of surface H^- vacancy, in which anionic electron is trapped ($H^- \rightarrow 1/2H_2 + e^-$). Since the formation of NH^{2-} vacancy is higher than that of H^- due to higher negative charge, the higher concentration of anion electrons at the anion vacancy is formed on Ca_2NH than CaNH, which reflects the difference in the catalytic performance between Ru/Ca_2NH and Ru/CaNH.

Figure 4b shows the dependence of the Ru-loading amount on the catalytic performance of Ru/Ca_2NH. The NH_3 synthesis rate increases significantly with the Ru loading and reaches an almost constant value (~3.5 mmol g^{-1} h^{-1}) at 2 wt % Ru. It can be considered that Ru nanoparticles are well dispersed up to 2 wt %, but the surface sites on Ca_2NH is almost occupied at 2wt% due to its low surface area (1.5 m^2 g^{-1}). Figure 4c compares the activities of various nitrides (surface area: 1–3 m^2 g^{-1}) supported Ru catalysts at 340 °C and 0.1 MPa. Ru/Li_3N and Ru/Mg_3N_2 have comparable catalytic activity to Ru/CaNH, and the other nitrides supported Ru catalysts show lower activity. On the other hand, Ru/Ca_2NH catalyst exhibited 5–80 times higher activity than the other catalysts, which suggests that the activity of Ru catalyst is effectively promoted by lattice H^- ions rather than lattice N^{3-} ions. The promotion effect of Ca_2NH support was further explored by N_2 isotopic exchange reaction ($^{15}N_2 + {}^{14}N_2 \leftrightarrow 2{}^{15}N{}^{14}N$) [20–22]. The N_2 dissociation ability of the catalyst can be evaluated the by $^{15}N^{14}N$ production rate. At 360 °C, the reaction rate of Ru/Ca_2NH is about 30 times higher than that of Ru/CaNH. Moreover, the activation energy of the former (59 kJ mol^{-1}) is almost half that of the latter (120 kJ mol^{-1}). It was thus demonstrated that N_2 dissociation is significantly facilitated by electron donation from Ca_2NH support to Ru.

Ammonia synthesis using isotopically labeled nitrogen ($^{15}N_2$) and hydrogen (D_2) was examined to clarify the reaction mechanism over Ru/CaNH. As shown in Fig. 5a, the signals with m/z = 19, 18, 17, and 16 increases with decreasing N_2 and D_2. Notably, the signals with m/z = 17 and 16 are much larger than the other signals during the initial reaction period (up to 3 h), meaning that NH_3 was preferentially generated over ND_3. From this observation, the following reaction mechanism can

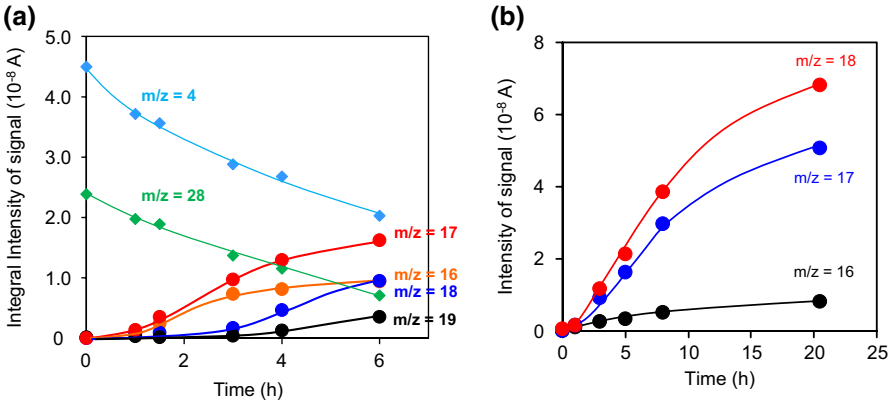

Fig. 5 **a** Reaction time profiles for ammonia synthesis from N_2 and D_2 over Ru/Ca_2NH at 340 °C. **b** Reaction time profiles for ammonia synthesis from $^{15}N_2$ and H_2 over Ru/Ca_2NH at 340 °C

be proposed. First, N_2 and D_2 are dissociated on Ru surface, and the N species on Ru reacts with H species in Ca_2NH to form NH_3, whereas D adatoms on Ru tend to be incorporated into the hydrogen vacancy of Ca_2NH. When Ru/Ca_2NH was heated in a mixture of $^{15}N_2$ and H_2, the signals with m/z = 18, 17, and 16 increased with the theoretical signal ratios ($^{15}NH_2(m/z=17)/^{15}NH_3(m/z=18)=0.8$ and $^{15}NH(m/z=16)/^{15}NH_3(m/z=18)=0.075$). Therefore, lattice nitrogen of Ca_2NH is not used in the ammonia synthesis reaction, which is contrary to the rare-earth metal nitride-based catalysts reported recently [23, 24]. These results suggest that ammonia synthesis over Ru/Ca_2NH proceeds through a lattice H^- ion-mediated Mars-van Krevelen (MvK) type mechanism [25–27] rather than the direct reaction of N and H adatoms on Ru surface (Langmuir–Hinshelwood mechanism). This MvK-type reaction mechanism was also confirmed by recent DFT calculations [28].

Comparison of catalytic performance of Ru/Ca_2N:e^- with Ru/Sr_2N:e^-

Sr_2N, a 2D electride with lower work function (~2.3 eV) than Ca_2N [29], was further evaluated as a support of Ru catalyst in ammonia synthesis. As shown in Fig. 6a, the initial ammonia synthesis rate is negligibly small, but the reaction rate increases steeply with reaction time and reaches a constant value of 1.35 mmol g^{-1} h^{-1} after 22 h. The total NH_3 produced from this reaction was roughly estimated to be 9 mmol, which is much higher than the mole of lattice nitrogen in Sr_2N (0.53 mmol) per 0.1 g of catalyst. Thus, the Ru/Sr_2N was found to be stable catalyst for NH_3 synthesis. The presence of Sr_2NH phase may prevent the aggregation of Ru particles through the Ru–N interaction as with the case of Ru/Ca_2NH [30], which accounts for the stable catalytic performance. The Sr_2N phase in Ru/Sr_2N catalyst is expected to be converted into Sr_2NH during the reaction as with the case of Ru/Ca_2NH. The apparent activation energy of Ru/Sr_2NH (58 kJ mol^{-1}) is almost identical to that of Ru/Ca_2NH (59 kJ mol^{-1}), implying

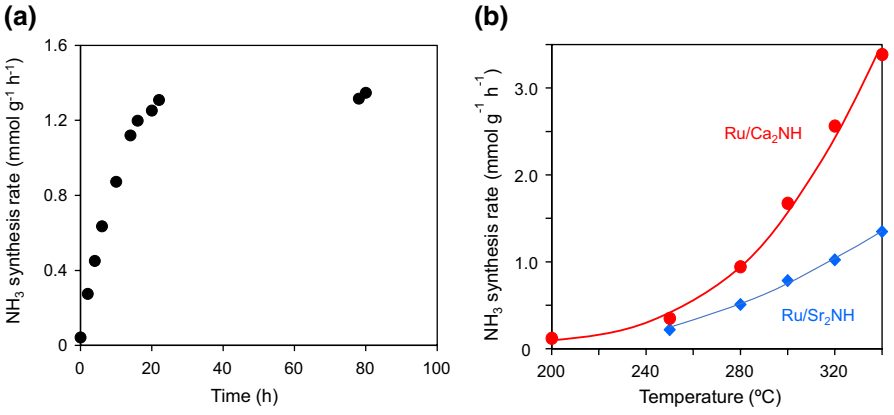

Fig. 6 **a** Reaction time profiles for ammonia synthesis over Ru/Sr_2N at 340 °C. **b** Temperature dependence of the rate of NH_3 synthesis over Ru/Ca_2NH and Ru/Sr_2NH catalysts at 0.1 MPa (WHSV, 36,000 mL g_{cat}^{-1} h^{-1})

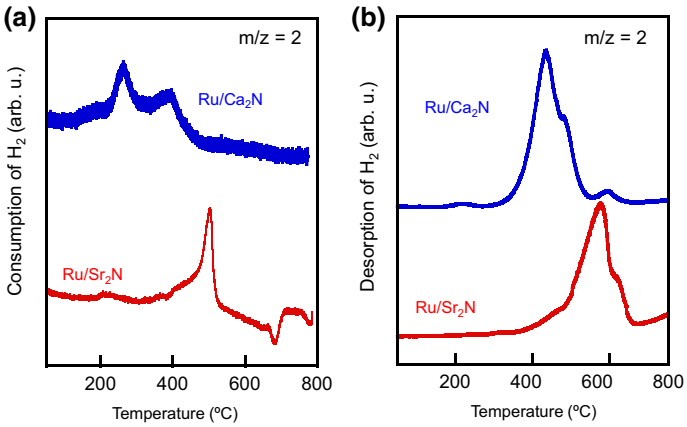

Fig. 7 **a** H_2-TPA profiles for Ru/Ca_2N and Ru/Sr_2N catalysts. **b** H_2-TPD profiles for Ru/Ca_2NH and Ru/Sr_2NH catalysts after NH_3 synthesis reaction at 340 °C for 10 h

that the reaction mechanism is very similar between these catalysts. However, the NH_3 synthesis rates of Ru/Sr_2NH is less than half that of Ru/Ca_2NH (Fig. 6b).

Temperature-programmed absorption (TPA) and desorption (TPD) of H_2 on these two catalysts were examined to clarify the difference in their catalytic performance. As shown in Fig. 7, both hydrogen absorption and desorption started at lower temperatures for Ru/Ca_2N as compared with Ru/Sr_2N. These observations come from hydrogen storage and release reaction at the interlayer space ($H^0 + e^- \leftrightarrow H^-$) and this reaction occurs reversibly during ammonia synthesis reaction. Hence, the formation of anionic electron at the H^- vacancy site promotes the N_2 dissociation to form NH_3 over these catalysts. H_2-TPA and TPD experiments revealed that hydrogen absorption–desorption capability of Ru/Sr_2NH is much lower than that of Ru/Ca_2NH below 400 °C, resulting that the density of anionic electrons formed on Ru/Sr_2NH catalyst is much inferior to that for Ru/Ca_2NH. Figure 8 shows the change in the

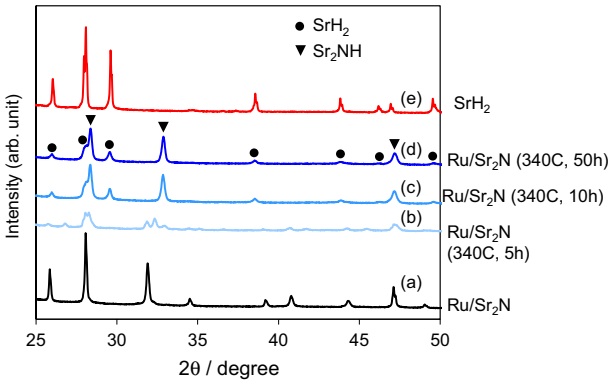

Fig. 8 XRD patterns for Ru/Sr_2N **a** before and after ammonia synthesis at 340 °C for **b** 5, **c** 10, and **d** 50 h. XRD pattern for SrH_2 is provided for reference

XRD patterns for Ru/Sr_2N with respect to reaction time. The Sr_2N phase was gradually converted into the mixture of Sr_2NH and SrH_2, that is, electrons between Sr_2N layers are partially replaced by H^- ions to form Sr_2NH and a part of Sr_2N framework is decomposed into SrH_2. It was therefore demonstrated that the framework structure of Sr_2N is relatively unstable for NH_3 synthesis than that of Ca_2N. Nevertheless, the Ru/Sr_2N catalyst has stable catalytic activity.

The role of lattice hydride and nitride on the catalytic performance

To investigate the effect of H^- ion on the activity of Ru catalyst for NH_3 synthesis, various metal hydrides are examined as a support for Ru catalyst. The catalytic activities of various hydrides supported Ru (2 wt%) catalysts are summarized in Fig. 9. Ru/Ca_2NH and Ru/Sr_2NH catalysts exhibited lower catalytic activity than Ru/CaH_2 and Ru/SrH_2, respectively. The difference in the catalytic activity may be ascribed to the density of H^- ions at Ru-support interface. More H^- ions are exposed on the surface for simple metal hydrides such as CaH_2 than for nitride-hydrides such as Ca_2NH. However, the activity of Ru/CaH_2 continuously decreases with reaction time (Fig. 10). On the other hand, Ru/Ca_2NH exhibited a stable NH_3 synthesis rate over long periods without degradation in activity. Transmission electron microscopy (TEM) analysis was conducted to investigate the microstructure of Ru nanoparticles on these catalysts during the reaction. As shown in Fig. 11, serious aggregation of Ru particles occurs for Ru/CaH_2 catalyst, where the mean particle size increases from 2.1 nm to 7.5 nm. In addition, it is reported that CaNH phase is slightly generated in Ru/CaH_2 catalyst during NH_3 synthesis [31]. Therefore, the Ru aggregation and CaNH formation leads to the decrease in the number of Ru-hydride interface, resulting in the deactivation of Ru/CaH_2 catalyst. In contrast, Ru nanoparticles with an average size of 2–3 nm are dispersed on Ca_2NH support and the Ru dispersion is maintained after the prolonged reaction (Fig. 11), which accounts for the high stability of catalytic activity.

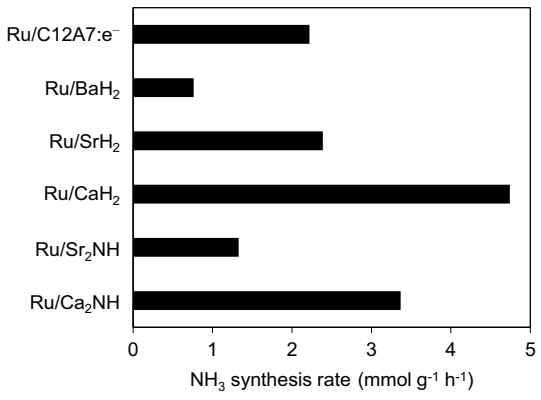

Fig. 9 NH_3 synthesis rate for various Ru catalysts at 340 °C and 0.1 MPa

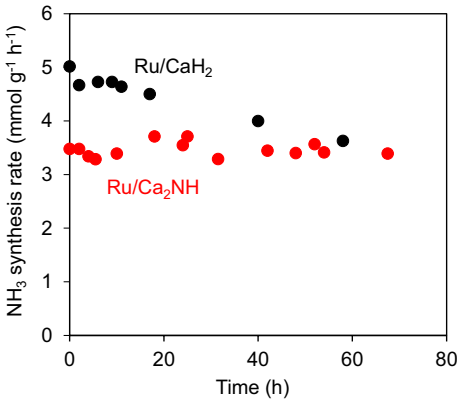

Fig. 10 Reaction time profiles for ammonia synthesis over Ru/CaH_2 and Ru/Ca_2NH at 340 °C and 0.1 MPa

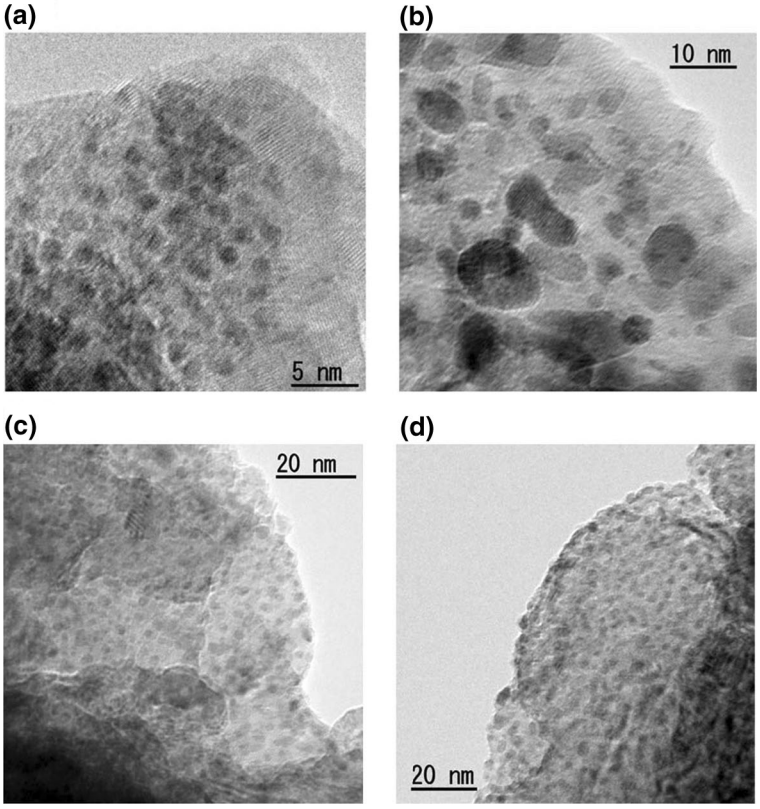

Fig. 11 TEM images of (**a**, **b**) Ru/CaH_2 and (**c**, **d**) Ru/Ca_2NH catalyst before and after ammonia synthesis. **a** and **c** are the images of each catalyst before reaction. **b** and **d** are the images of each catalyst after reaction at 340 °C for 50 hs

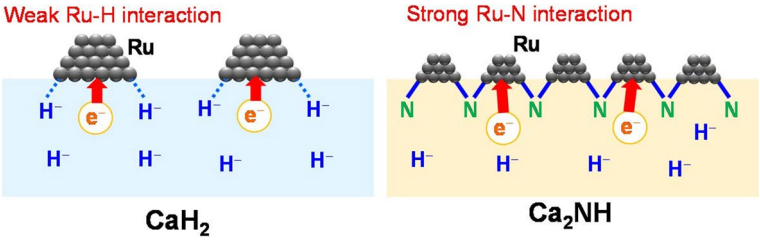

Fig. 12 Schematic illustration of Ru/Ca_2NH and Ru/CaH_2 catalysts

The difference in the catalytic performance between Ru/Ca_2NH and Ru/CaH_2 can be explained based on Fig. 12. In the case of Ru/CaH_2, high density H^- ions are exposed on the surface of CaH_2, resulting that a number of anionic electrons with low work function (~2.7 eV) are generated at H^- ion vacancy sites [32]. As a consequence, N_2 dissociation reaction over Ru is promoted by electron donation from the CaH_2 support, which is attributed to the high catalytic activity at the initial stage of the reaction. However, weak interaction between Ru and H^- ion causes the aggregation of Ru nanoparticles during the reaction, leading to the degradation of the catalytic activity. As for Ru/Ca_2NH, the concentration of H^- ions at Ru-support interface is lower than that for Ru/CaH_2 catalyst, but Ru nanoparticles are immobilized on the Ca_2NH surface through the strong Ru–N interaction. Hence, the high and stable catalytic performance is realized for Ru/Ca_2NH catalyst.

Conclusions

The present study demonstrates that calcium-based nitride hydride, Ca_2NH, can work as an efficient and stable supports for Ru catalysts in ammonia synthesis. Ru-loaded Ca_2NH exhibits much higher catalytic activity than various nitride-supported Ru catalysts and Ru/Sr_2NH with the same crystal structure as Ru/Ca_2NH. The strong $Ru-N$ bonding on the Ru/Ca_2NH catalyst works to anchor the Ru nanoparticles to the Ca_2NH support, resulting in the stable catalytic performance by suppression of agglomeration of the Ru nanoparticles. The present finding reveals that strong electron-donating ability derived from low work function electron formed at H^- ion vacancy sites as well as strong Ru-support interaction plays a crucial role in high catalytic performance of Ru/Ca_2NH.

Memory with Prof. Michel Che

(M.K.) I met Prof. Michel Che for the first time at his lecture held at Osaka Prefecture University when I was a PhD student of Prof. Anpo's laboratory. I was very impressed with his research activity and his approach to understand catalytic process from the molecular level using various spectroscopic techniques. And I remember that he answered my poor English questions politely and kindly. Unfortunately, I

couldn't have the opportunity to discuss with Prof. Michel Che about my research work after I obtained a PhD, but he is my goal as a researcher.

(H.H.) I learned a lot from his review article on active oxygen species oxide surfaces published in 1982. This knowledge led to the discovery of the formation of superoxide radical anion in $12CaO•7Al_2O_3$ (C12A7) (Inorg.Chem.1982), which triggered the extensive research on C12A7 including the first RT stable electride materials (Science 2003).

Acknowledgements This work was supported by a grant from the Element Strategy Initiative to Form Core Research Center (No. JPMXP0112101001) of the Ministry of Education, Culture, Sports, Science and Technology of Japan (MEXT), a PRESTO Grant (No. JPMJPR18T6) from the Japan Science and Technology Agency (JST) and Kakenhi Grants-in-Aid (Nos. 17H06153, JP19H05051 and JP19H02512) from the Japan Society for the Promotion of Science (JSPS).

References

1. T. Kandemir, M.E. Schuster, A. Senyshyn, M. Behrens, R. Schlögl, Angew. Chem. Int. Ed. **52**, 12723 (2013)
2. L. Wang, M.K. Xia, H. Wang, K.F. Huang, C.X. Qian, C.T. Maravelias, G.A. Ozin, Joule **2**, 1055 (2018)
3. Y. Niwa, K. Aika, Res. Chem. Intermed. **24**, 593 (1998)
4. K. Aika, A. Ozaki, H. Hori. J. Catal. **27**, 424 (1972)
5. F. Rosowski, A. Hornung, O. Hinrichsen, D. Herein, M. Muhler, G. Ertl, Appl. Catal. A **151**, 443 (1997)
6. T.W. Hansen, J.B. Wagner, P.L. Hansen, S. Dahl, H. Topsoe, C.J.H. Jacobsen, Science **294**, 1508 (2001)
7. H. Bielawa, O. Hinrichsen, A. Birkner, M. Muhler, Angew. Chem. Int. Ed. **40**, 1061 (2001)
8. N. Saadatjou, A. Jafari, S. Sahebdelfar, Chem. Eng. Commun. **202**, 420 (2015)
9. K. Aika, Catal. Today **286**, 14 (2017)
10. S.E. Siporin, R.J. Davis, J. Catal. **225**, 359 (2004)
11. M. Kitano, Y. Inoue, Y. Yamazaki, F. Hayashi, S. Kanbara, S. Matsuishi, T. Yokoyama, S.W. Kim, M. Hara, H. Hosono, Nat. Chem. **4**, 934 (2012)
12. M. Kitano, S. Kanbara, Y. Inoue, N. Kuganathan, P.V. Sushko, T. Yokoyama, M. Hara, H. Hosono, Nat. Commun. **6**, 6731 (2015)
13. S. Kanbara, M. Kitano, Y. Inoue, T. Yokoyama, M. Hara, H. Hosono, J. Am. Chem. Soc. **137**, 14517 (2015)
14. M. Kitano, Y. Inoue, H. Ishikawa, K. Yamagata, T. Nakao, T. Tada, S. Matsuishi, T. Yokoyama, M. Hara, H. Hosono, Chem. Sci. **7**, 4036 (2016)
15. K. Lee, S.W. Kim, Y. Toda, S. Matsuishi, H. Hosono, Nature **494**, 336 (2013)
16. S. Matsuishi, Y. Toda, M. Miyakawa, K. Hayashi, T. Kamiya, M. Hirano, I. Tanaka, H. Hosono, Science **301**, 626 (2003)
17. P. Chen, Z.T. Xiong, J.Z. Luo, J.Y. Lin, K.L. Tan, J. Phys. Chem. B **107**, 10967 (2003)
18. G.T. Wu, Z.T. Xiong, T. Liu, Y.F. Liu, J.J. Hu, P. Chen, Y.P. Feng, A.T.S. Wee, Inorg. Chem. **46**, 517 (2007)
19. F. Hayashi, Y. Tomota, M. Kitano, Y. Toda, T. Yokoyama, H. Hosono, J. Am. Chem. Soc. **136**, 11698 (2014)
20. Y. Morikawa, A. Ozaki, J. Catal. **12**, 145 (1968)
21. O. Hinrichsen, F. Rosowski, A. Hornung, M. Muhler, G. Ertl, J. Catal. **165**, 33 (1997)
22. T. Hikita, Y. Kadowaki, K.I. Aika, J. Phys. Chem. **95**, 9396 (1991)
23. M. Kitano, J. Kujirai, K. Ogasawara, S. Matsuishi, T. Tada, H. Abe, Y. Niwa, H. Hosono, J. Am. Chem. Soc. **141**, 20344 (2019)
24. T.N. Ye, S.W. Park, Y. Lu, J. Li, M. Sasase, M. Kitano, T. Tada, H. Hosono, Nature **583**, 391 (2020)
25. P. Mars, D.W. van Krevelen, Chem. Eng. Sci. **3**, 41 (1954)

26. F. Zasada, J. Janas, W. Piskorz, Z. Sojka, Res. Chem. Intermed. **43**, 2865 (2017)
27. S.W. Hoh, L. Thomas, G. Jones, D.J. Willock, Res. Chem. Intermed. **41**, 9587 (2015)
28. T. Nakao, T. Tada, H. Hosono, J. Phys. Chem. C **124**, 2070 (2019)
29. W. Ming, M. Yoon, M.H. Du, K. Lee, S.W. Kim, J. Am. Chem. Soc. **138**, 15336 (2016)
30. H. Abe, Y. Niwa, M. Kitano, Y. Inoue, M. Sasase, T. Nakao, T. Tada, T. Yokoyama, M. Hara, H. Hosono, J. Phys. Chem. C **121**, 20900 (2017)
31. M. Hattori, T. Mori, T. Arai, Y. Inoue, M. Sasase, T. Tada, M. Kitano, T. Yokoyama, M. Hara, H. Hosono, ACS Catal. **8**, 10977 (2018)
32. P.-V. Ong, L.E. Johnson, H. Hosono, P.V. Sushko, J. Mater. Chem. A **5**, 5550 (2017)